

Article

Matrix-Assisted Processes in CH₄-Doped Ar Ices Irradiated with an Electron Beam

Mykhailo Bludov, Ivan Khyzhniy, Sergey Uyutnov and Elena Savchenko *

B. Verkin Institute for Low Temperature Physics & Engineering NASU, 61103 Kharkiv, Ukraine; m.bludov@ilt.kharkov.ua (M.B.); khyzhniy@ilt.kharkov.ua (I.K.); uyutnov@ilt.kharkov.ua (S.U.)

* Correspondence: elena.savchenko@gmail.com

Abstract: The relaxation processes induced by exposure of the Ar matrices doped with CH₄ (0.1–10%) to an electron beam were studied with a focus on the dynamics of radiolysis products—H atoms, H₂ molecules, CH radicals, and energy transfer processes. Three channels of energy transfer to dopant and radiolysis products were discussed, including free charge carriers, free excitons and photons from the “intrinsic source” provided by the emission of the self-trapped excitons. Radiolysis products along with the total yield of desorbing particles were monitored in a correlated manner. Analysis of methane transformation reactions induced by free excitons showed that the CH radical can be considered a marker of the CH₃ species. The competition between exciton self-trapping and energy transfer to the dopant and radiolysis products has been demonstrated. A nonlinear concentration behavior of the H atoms in doped Ar matrices has been established. Real-time correlated monitoring of optical emissions (H atom and CH₃ radicals), particle ejection, and temperature revealed a nonmonotonic behavior of optical yields with a strong luminescence flash after almost an hour of exposure, which correlated with the explosive pulse of particle ejection and temperature. The connection of this phenomenon with the processes of energy transfer and recombination reactions has been established. It is shown that the delayed explosive ejection of particles is driven by both the recombination of H atoms and CH₃ radicals. This occurs after their accumulation to a critical concentration in matrices at a CH₄ content $C \geq 1\%$.

Keywords: solid methane; astrophysical ices; matrix isolation; electron irradiation; radiolysis; energy transfer; particle ejection; relaxation processes; luminescence



Citation: Bludov, M.; Khyzhniy, I.; Uyutnov, S.; Savchenko, E.

Matrix-Assisted Processes in CH₄-Doped Ar Ices Irradiated with an Electron Beam. *Methane* **2023**, *2*, 372–388. <https://doi.org/10.3390/methane2040025>

Academic Editor: Patrick Da Costa

Received: 31 July 2023

Revised: 25 August 2023

Accepted: 11 September 2023

Published: 7 October 2023



Copyright: © 2023 by the authors. Licensee MDPI, Basel, Switzerland. This article is an open access article distributed under the terms and conditions of the Creative Commons Attribution (CC BY) license (<https://creativecommons.org/licenses/by/4.0/>).

1. Introduction

Radiation effects in solid methane and methane-containing frozen films, so-called ices, attract much attention in diverse fields of science and technology. Being widely present in the universe [1–6], methane plays an important role in astrophysics and astrochemistry [7]. An overview of laboratory experiments on the relationship of methane to prebiotic chemistry is presented in [8]. The properties of methane, their transformation caused by the continuous radiation of outer space, and physico-chemical processes became the topic of a large body of research. Numerous efforts have been made to simulate radiation-induced processes in the laboratory using a variety of techniques surveyed in Ref. [9]. Various types of ionizing radiation were used to study the radiation behavior of methane and methane-rich ices—ions [10–19], electrons [20–29] and photons [26,30–35].

The interaction of solid methane with neutrons is closely connected to the technology of cryogenic moderators [36–42]. Solid methane is widely used for moderating hot neutrons to cold and ultra-cold ones because its efficiency is approximately 3.5 times that of the commonly used liquid hydrogen-based moderator [36]. Despite the attractive neutronic properties of solid methane, its use in cryogenic moderators faces a problem, especially for high-intensity neutron fluxes. After long exposure to neutron radiation, as it was found by Carpenter [36,37], solid methane moderators experienced sudden, violent warm-ups

and pressure rises in their vessels, in some cases with followed vessel destruction. This phenomenon, called the “burp” effect, significantly constrains the current use of solid methane moderators. The reason for this phenomenon, according to [36,37], is a large spontaneous release of energy. The moderator material stores a part of the energy absorbed from radiation in view of frozen-in products of radiolysis. At a high density of reactive species, their recombination and the expansion of hydrogen, which builds up in the solid methane during irradiation by neutrons [36], result in fast energy release, which destroys a moderator vessel. The pressing character of this problem stimulated the thorough study of the interaction of neutron radiation with solid methane [37,38,40–42]. According to Carpenter’s model [37], all recombination processes in solid methane moderators proceed in one stage and are controlled by the same activation energy for defect diffusion. However, commissioning tests of the ISIS TS2 solid methane moderator, in which a “burp”-like effect was observed [40], and the study of relaxation phenomena in solid methane pre-irradiated with an electron beam [28], led to the conclusion that the radiolysis defect recombination process happens in two stages, at different temperatures, and is therefore controlled by two different activation energies. Modifying Carpenter’s approach, Kirichek and coauthors implemented two different types of radiation defects (H atoms and CH₃ radicals), with different recombination rates and thermal activation energies [40]. The suggested model satisfactorily described results of the commissioning tests of the ISIS TS2 solid methane moderator. The possible role of radiolysis product recombination processes in cryo-volcanism on comets was discussed in [37,40].

Strong explosive-like delayed ejection of particles was observed in solid methane exposed to an electron beam of the subthreshold energy [29,43]; that is, under conditions when the impact mechanisms of defect formation and desorption are excluded. The effect was observed at a low temperature upon reaching a critical irradiation dose of 100 eV per methane molecule and was accompanied by the sample temperature rise and a flash of luminescence. The outburst of particles was preceded by oscillations of particle ejection with increasing amplitude. The period of these oscillations depended on the intensity of the irradiation, it decreases with an increase in the beam current density. In [44], a model has been proposed that qualitatively describes the appearance of two types of self-oscillations upon electronic excitation of solid CH₄, their periods and the delay time of burst. Two types of self-oscillations found are a periodic change of temperature and concentration with time of CH₄ decay products—H atoms and CH₃ radicals upon irradiation. The found patterns of self-oscillations were shown to determine the temporal dynamics of the delayed explosive particle ejection upon irradiation with the subthreshold electrons. The discovered effect is a new manifestation of self-oscillations similar to those considered in [45]. To the best of our knowledge, there were only a few studies in which a delayed-in-time burst of particles, the so-called “delayed desorption”, from solid methane exposed to other types of ionizing radiation, was observed [46,47]. In [46], solid CD₄ was irradiated with MeV He⁺ and H⁺. When the beam was turned on, weak desorption of D₂ first appeared. Upon reaching the threshold fluence density, the yield of D₂ rapidly increased by more than an order of magnitude, and then gradually decreased. The threshold fluence values for irradiation with 1.5 MeV He⁺ ions and 1.5 MeV H⁺ were 3×10^{14} ions cm⁻² and 9×10^{15} ions cm⁻², respectively. In [47], solid CH₄ and CD₄ were irradiated with 9.0 MeV α particles and 7.3 MeV protons. Doses up to 145 eV caused pressure shocks, raising the chamber pressure by several orders of magnitude. This process released up to 90% of the molecules of the solid target into the gas phase. The authors concluded that the H and CH₃ radicals play a major role in this phenomenon, and the observed explosion resembles a non-equilibrium process. However, in these experiments, no regular oscillations were observed. The detection of complex organic molecules (COMs) in the gas phase of cold molecular clouds at such low temperatures of the cryogenic environment that they would have to condense on the surfaces raised the question of the reasons for this phenomenon. Several hypotheses have been proposed [48–52] and radical–radical-induced explosive desorption of ice-coated interstellar nanoparticles is among them [52]. In this article, the authors

present the direct observation by Fourier transform infrared (FTIR) spectroscopy of rapid radical–radical reactions of formyl (HCO•) and methyl (•CH₃) radicals and the reaction-induced explosive desorption during the exposure of methane and carbon monoxide ices to superthreshold 5 keV electrons. However, the formation and recombination of the H atom remained beyond the reach of this experimental approach.

To get more insight into the phenomenon, the matrix isolation method was introduced, in combination with a set of emission spectroscopy methods [53–55]. It should be noted that in contrast to pure methane and mixtures of methane with other molecular gases of astrophysical interest, there are only a few studies performed in matrices of rare gases [56–58]. Photolysis of methane in Kr matrix was studied using synchrotron radiation [56]. Strong VUV absorption and emission features were attributed to atomic carbon C and the CH radical. Neither CH₂ nor CH₃ were observed in the Kr matrix. In contrast to that, photolysis of methane in the Ne matrix resulted in the appearance of a wide range of hydrocarbons, including CH₃ and carbon clusters C_n with a number of atoms up to n = 20 [58].

Below, we briefly summarize the results of our previous studies of radiation effects induced by an electron beam in Ar matrices doped with CH₄ [53–55,59]. In the cathodoluminescence (CL) spectra, the following products of radiation-induced methane transformation were recorded: H, CH and C. It has been shown that because of the small penetration depth of electrons, the bulk of the matrix is excited preferentially by photons of the matrix with an energy of 9.8 eV (the most intense emission band of the self-trapped excitons); in other words, “internal photolysis” occurs. Analysis of the efficiency of different channels of methane transformation under these photons and neutralization reactions indicated that the CH radical can be considered a signature of the CH₃ radicals [55]. Monitoring of the so-called nonstationary luminescence (NsL), viz. luminescence under nonstationary conditions (upon external heating under beam) in combination with the detection of thermally stimulated exoelectron emission (TSEE), and optical emission spectroscopy made it possible to reveal the contribution of the reactions of charged and neutral species. The dynamics of the main products of methane fragmentation were traced and it was found that the behavior of CH radicals (therefore, CH₃ radicals) and hydrogen atoms is different and depends on the concentration of methane in the matrix. This means that the assumption about the same concentration of CH₃ radicals and H atoms based only on the reaction, CH₄ + ΔE → CH₃ + H, accepted in the delayed explosive desorption models [37,40,44], is not entirely correct. Long-term and short-term oscillations of the total particle yields were found and interpreted as thermo-concentration self-oscillations, similar to those considered in [44] for the case of pure methane. It has been shown that they can be initiated either by the spontaneous release of stored energy upon reaching a critical concentration of reactants, or by external heating of the doped matrix to stimulate diffusion and release the stored chemical energy in subsequent recombination reactions [59]. Preliminary measurements of the dose dependence of the optical emission of the H atom carried out on a lightly doped Ar matrix (C = 1%) at LHe temperature found a puzzling fact—an increase in this emission with a pressure burst [54]. The dynamics of optical emissions from highly doped matrices upon low-temperature irradiation remained unexplored.

Here, we present an outgrowth of this research with a focus on H atom and CH₃ radical behavior at different concentrations of CH₄ in the Ar matrix and processes induced by energy transfer from the matrix to dopant and products of radiolysis. The choice of the matrix made it possible to implement the selective excitation of methane impurities and radiolysis products. Three channels of energy transfer are considered—charge transfer (by holes), transfer by free excitons and self-trapped excitons. Special attention is paid to the recombination of H atoms and its monitoring in the matrix. This reaction proceeds nonradiatively with an energy release of 218 kJ mole^{−1}. A hydrogen molecule can be monitored by being transferred to an excited state. The thresholds of excitation of the lowest singlet (B¹Σ_u⁺) and triplet (a³Σ_g⁺) excited states [60] are below the bands of free excitons of Ar—12.06 eV for Γ(3/2) and 12.24 eV for Γ(1/2) [61]. So, the transfer of energy by free excitons to the hydrogen molecule can lead to its transition to the lowest

excited states $B^1\Sigma_u^+$ and $a^3\Sigma_g^+$. Electric dipole transitions from the coupled triplet state $a^3\Sigma_g^+$ into an unstable lower state $b^3\Sigma_u^+$ lead to the appearance of a wide emission continuum [62] followed by dissociation of the H_2 molecule. The detection of H atoms proceeds under conditions of competition between exciton self-trapping and energy transfer to the dopant and radiolysis products. A nonlinear concentration behavior of the optical emission of H atoms in doped Ar matrices has been found. Real-time correlated monitoring of optical emissions (H atom and CH_3 radicals), particle ejection, and temperature revealed a nonmonotonic behavior of optical yields with a strong luminescence flash after almost an hour of exposure, which correlated with the surge of temperature and particle ejection. The connection of this phenomenon with the processes of energy transfer and recombination reactions has been established. It is shown that the delayed explosive ejection of particles is driven by both the recombination of H atoms and CH_3 radicals. The study of charge accumulation in pure Ar, CH_4 -doped Ar, and pure methane by the TSEE method ruled out the “Coulomb explosion” scenario as the underlying mechanism of delayed explosive ejection of particles under the beam.

2. Experimental

2.1. Choice of Matrix

The electronically excited states of CH_4 are of a dissociative nature, and any kind of irradiation will lead to the appearance of radiolysis products in the spectra. The Ar matrix ensures effective excitation of the dopant, since free and self-trapped Ar excitons fall into the region of the absorption band of the CH_4 molecule [63], as shown in Figure 1.

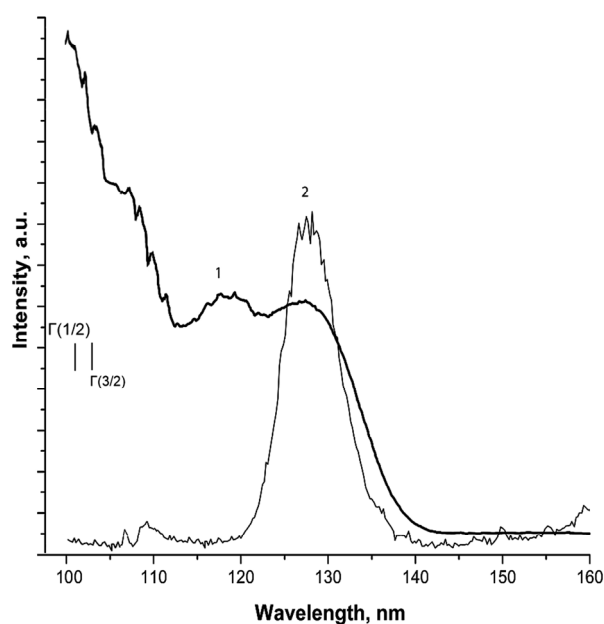


Figure 1. Comparison of the most intense emission band of Ar matrix (curve 2) with the absorption cross-section of gaseous CH_4 (curve 1), adopted from [63].

The Ar matrix is transparent to the radiation of self-trapped excitons (the most intense radiation of the matrix) since these states lie below the intrinsic absorption threshold of the matrix, which makes it possible to effectively excite the methane molecule throughout the volume, stimulating its dissociation through photon processes. It is worth noting that the energies of free and self-trapped excitons in solid Ar (12.06 and 9.8 eV, respectively) are close to the photon energy of the most intense line in the VUV solar spectrum (Lyman- α), and the study of excitation induced processes in an Ar matrix is of interest for planetary astrochemistry. The second reason for choosing solid Ar as a matrix is the high ionization potential I of Ar ($I = 15.76$ eV) [64], which exceeds the ionization potential of methane itself and its radiation-induced transformation products, as shown in Table 1.

Table 1. Ionization potentials and electron affinities of methane and products of its transformation.

Species	Ionization Potential, eV	Electron Affinity, eV
CH ₄	12.61	unstable
CH ₃	9.84	+0.09
CH ₂	10.35	+0.65
CH	10.64	+1.24
H	13.59	+0.75
H ₂	15.43	unstable
C	11.26	1.26

The data are presented according to [64].

This choice ensures charge transfer from the matrix to the dopant as well as to the radiolysis products and prevents the reverse process of charge transfer from CH₄⁺ and other cations to the matrix. The third reason for the choice is related to geometric parameters. The methane molecule with a kinetic diameter of 0.380 nm [65] can occupy the substitutional site in the Ar matrix which is about 0.376 nm [66]. When a methane concentration increases to 3%, the Ar lattice in the vicinity of the dopant begins to modify, and, at a higher concentration of about 20%, a two-phase system is obtained [67].

2.2. Sample Preparation and Control

The experimental procedures have been described in detail in [53]. Here, we give a brief account of the procedures. We used Ar gas (99.998%) and CH₄ gas (99.97%) without further purification. The mixture of Ar and CH₄ of the chosen concentration was performed in the gas-handling system, which was heated and degassed before each experiment. In these experiments, we worked in the range of methane concentrations from 0.1 to 10%. Films of solid Ar doped with methane were grown by deposition of a certain amount of premixed gas of room temperature onto a cooled to LHe temperature oxygen-free Cu substrate mounted in a high-vacuum chamber with a base pressure of <10⁻⁷ torr. Pumping out was carried out by LHe cryogenic pump and magnetic discharge pump. All measurements, both while the beam is on, and after its shutdown and subsequent heating, were performed in the dynamic pumping out mode. The pressure in the experimental chamber was monitored throughout the entire experiment. Films of the same thickness (25 μm) grown in the same mode were used for all concentrations. They were fairly transparent which indicated their good structural properties and did not require annealing. The presence of impurities was controlled spectroscopically. The sample temperature was monitored during the entire experiment with a Si sensor mounted on the substrate.

To obtain some information about the structural features of the grown and irradiated samples and electron accumulation in shallow traps, we measured the thermally stimulated exoelectronic emission (TSEE) from all preliminarily irradiated in identical way doped matrices as well as pure Ar and methane. The irradiation was performed with a subcritical dose. In these experiments, we used heating with a constant rate of 5 K min⁻¹. Measurements of TSEE were started after decaying of the “afteremission” current to zero. Electrons released from shallow traps (defects of structure) upon heating can either neutralize cations or escape from the film yielding a TSEE current. Stimulated currents were detected with an electrode kept at a small positive potential V_F = +9 V and connected to the current amplifier. Measurements of the TSEE yields were carried out in the temperature range of 5–50 K.

2.3. Irradiation Mode and Optical Emission Measurements

The reason for choosing electrons as projectiles is that electrons are common secondary particles under any kind of irradiation and the results obtained in this way can be applied to the wider field of radiation physics. Irradiation was carried out by electrons with subthreshold energy ($E_e < 1.7$ keV) to exclude the formation of defects and sputtering of samples via the impact mechanism, while the mechanisms of electronically stimulated defect formation and desorption operate. In these experiments, the electron beam energy E_e

was set to 1.5 keV with a current density of 2.5 mA cm^{-2} . The electron gun was operating in the dc regime under controlled conditions. The beam covered the icy film surface with an area of 1 cm^2 . The sample heating when turning on the electron beam did not exceed 0.4 K. All measurements of spectral features were carried out at 5 K. The open surface of the samples enabled us to measure cathodoluminescence (CL) spectra not only in visible but also in the vacuum ultraviolet (VUV) range, as well as to measure the TSEE yields as described before. The dose deposited by irradiation was determined from the exposure time for a constant beam intensity. The dose dependencies of spectrally resolved features were measured simultaneously with constant monitoring of desorption processes by the chamber pressure recording with an ionization detector (a Bayard-Alpert gauge). Note, that all measurements were performed in the dynamic pumping-out mode.

3. Results and Discussion

It is interesting to compare the TSEE yields from a pure Ar matrix with the TSEE yields from CH_4 -doped matrices and pure methane. Due to the high mobility of electrons in solid Ar and methane [68], TSEE monitoring makes it possible to obtain information on relaxation processes not only near the surface, but also in the bulk of the matrix. The TSEE yields measured reflect the distribution of electron traps (defects) in the sample and provide information on the defects of growth and radiation-induced ones, as well as charge accumulation and the temperature ranges in which the neutralization processes will occur. Figure 2 illustrates TSEE yields from pure Ar, doped Ar matrices and pure CH_4 .

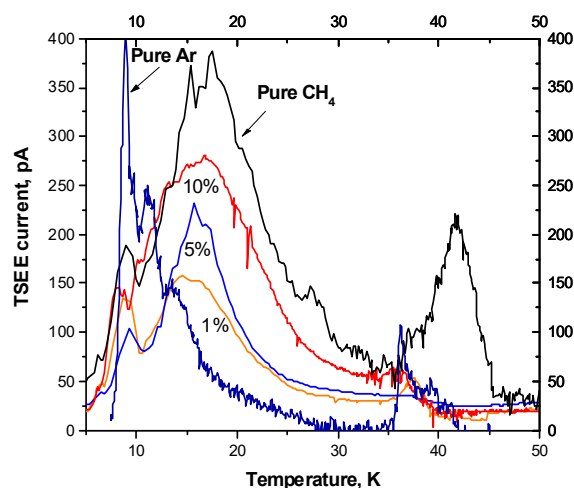


Figure 2. TSEE yields recorded from pre-irradiated CH_4 , CH_4 -doped Ar matrices and pure Ar.

The low-temperature peak at 8 K in the doped samples coincides with that recorded in the pure Ar matrix, but has a much lower intensity. The decrease in its intensity in doped matrices may be connected with a change of trap distribution in favor of deep ones due to the attachment of an electron to some radiolysis products with a positive electron affinity (see Table 1). The next wide feature at about 16 K represents a multipeak curve with unresolved structure incorporating components related to different defects of structure. The shape of these curves is similar for all doped samples and similar to that of the pure methane. The intensity of this feature increases with the growth of methane concentration. This suggests that this feature is related to defects induced by the incorporation of methane molecules and radiolysis products into the Ar matrix and possible methane cluster formation. An important point is the fact that the number of electrons accumulated in shallow traps of the Ar matrix doped with 1% CH_4 is almost the same as in the matrix of pure Ar, while explosive delayed desorption was not observed in pure solid Ar, in contrast to the doped Ar matrices. This fact rejects the Coulomb explosion model for this phenomenon.

As already mentioned, the electronic states of the methane molecule are dissociative, so its luminescence spectrum is determined by the products of its radiolysis. The main

channels of CH₄ degradation upon photon flux with the threshold wavelengths [69] in the solid Ar emission range are:



In accordance with this, we detected the following emissive products of methane degradation: H, CH, C and H₂, as can be seen from the CL spectrum shown in Figure 3.

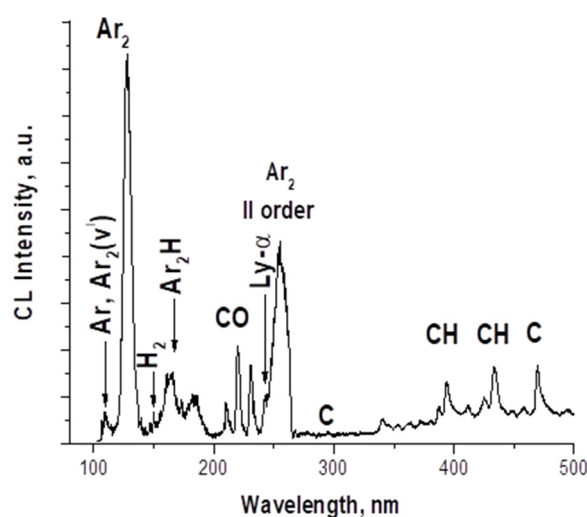


Figure 3. CL spectrum of solid Ar doped with 1% CH₄ taken upon irradiation at 5 K.

The spectrum contains both the emission bands of the matrix and the emission bands of the radiolysis products. Emissions are observed both from the solid phase and the gaseous phase due to electronically induced desorption. The most intense feature of this spectrum at 127 nm is the well-known emission of the molecular-type self-trapped excitons (STE)—Ar₂^{*}, corresponding to bound-free transitions from the ^{1,3}Σ_u⁺ states to the repulsive part of the ground state ¹Σ_g⁺ [61]. At the short-wavelength edge of the Ar₂^{*} band, recorded in the second order, the Lyman-α line, which belongs to the desorbed into the gas phase excited H atoms, was detected. H atoms in the matrix manifest themselves by Ar₂H excimer band at 166 nm [70]. Mechanisms of the excited H atoms formation and their desorption from Ar matrices, doped with CH₄, were discussed recently [71]. Four scenarios for the desorption of excited H atoms were proposed, including energy transfer by holes and excitons of the Ar matrix. Own atoms of the matrix and molecules also desorb in excited states emitting the corresponding lines and band (a feature with an unresolved structure in Figure 3). Their desorption is driven by the exciton mechanism [72]. A necessary condition of the electronically stimulated desorption is the localization of electronic excitation on the atoms or molecules in the near-surface region with the release of energy exceeding the binding energy per atom ε_b (for an atom of Ar matrix ε_b = 88.8 meV [61]). For the case of the Ar matrix desorption of excited particles (including H^{*} atoms) is facilitated by negative electron affinity of Ar χ = −0.4 eV [61], in other words, excited particles are ejected under the repulsive forces between an excited atom and atoms of surrounding lattice, so-called “cavity-ejection” mechanism [72]. Interestingly, the desorption of excited argon

molecules in the states $1,3\Sigma_u^+(v')$ was also detected as a result of a self-trapped hole (Ar_2^+) neutralization reaction [73]. The so-called “third continuum” of Ar at 200 nm, assigned to radiative transitions from the excited $(\text{Ar}_2^+)^*$ state [74], was quenched by an admixture of methane. Note that the Ar_2^* -band recorded in the second order overlaps with a wide emission continuum of molecular hydrogen associated with transitions from the bound triplet state $a^3\Sigma_g^+$ to the unstable lower state $b^3\Sigma_u^+$, which makes it difficult to monitor the H_2 molecule by this transition. According to [75], the maximum spectral distribution of the radiative transition probability from the level $v' = 0$ of the term $a^3\Sigma_g^+$ is about 260 nm. A weak band at 146 nm observed in the CL spectrum was tentatively assigned to the band 0–6 of the Lyman series $\text{B}^1\Sigma_u^+ \rightarrow \text{X}^1\Sigma_g^+$ of molecular hydrogen. However, it was not possible to use this band for the H_2 monitoring because of its low intensity. In the visible range, we detected emission bands of other radiolysis products—CH radical and C atom. CH radicals were registered by the emission bands at 432 nm (the $\text{A}^2\Delta \rightarrow \text{X}^2\Pi$ transition) and 387 nm (the $\text{B}^2\Sigma^- \rightarrow \text{X}^2\Pi$ transition). C atoms were recorded by the emission lines at 470 nm (the $^1\text{S} \rightarrow ^3\text{P}$ transition) and 295 nm (the $^5\text{S}^0 \rightarrow ^3\text{P}$ transition). The spectrum also contains a broad band at 184 nm unidentified at present and impurity bands of CO (the Cameron system $a^3\Pi \rightarrow \text{X}^1\Sigma^+$).

The positions and half-widths of the observed bands remain practically unchanged over the entire concentration range studied. The main changes in the spectra relate to changes in the relative intensity of bands. Upon doping of Ar matrices, a strong quenching of the emission band of self-trapped excitons (that is the M-band) was observed as shown in Figure 4.

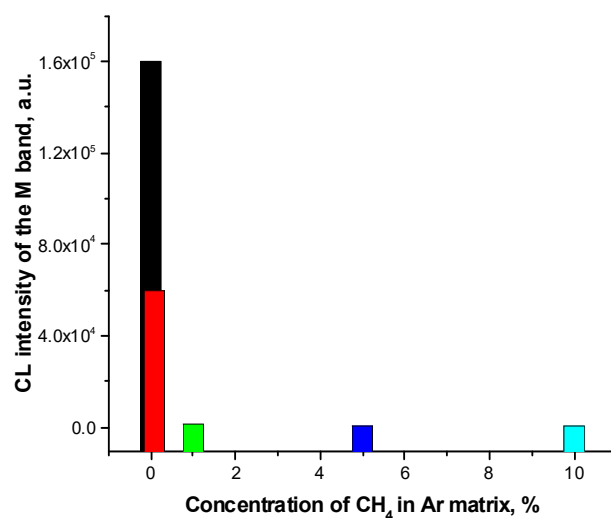


Figure 4. Intensity of the M-band in pure Ar (first black column) and in CH_4 -doped Ar matrices.

This demonstrates quite efficient energy transfer by free excitons to dopant and radiolysis products, since the diffusion length L_{dif} of thermalized free excitons in solid Ar ($L_{\text{dif}} \sim 100$ nm [76,77]) exceeds the distance between the dopants already at $C = 0.1\%$.

H atoms in the matrices were traced by a CL band centered at 166 nm, which belongs to the excimer Ar_2H^* [70]. Formation of Ar_2H^* occurs with the participation of the matrix hole Ar^+ at the expense of the large affinity of Ar atom to a proton (proton affinity PA—369.2 kJ mol^{-1} [64]). The quantum chemical calculations [78] on the Rg_nH^+ species showed that the configuration with two solvent atoms of the $\text{D}_{\infty h}$ configuration with a proton between them is the energetically favorable configuration of the proton solvated in all rare gas matrices. The recombination of Ar_2H^+ cations with electrons results in the appearance of the excimers Ar_2H^* . It is interesting to follow the change in the relative intensity of this excimer band with the dopant concentration. The intensity of the Ar_2H^* emission band, hereinafter referred to as H, measured with respect to the Ar_2 band of self-trapped excitons, denoted as M, is shown in Figure 5.

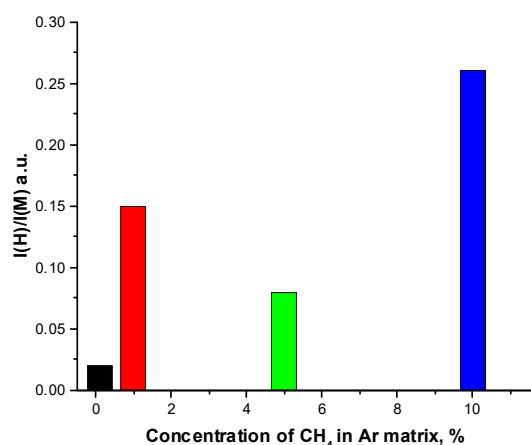


Figure 5. The relative intensity of the Ar₂H* (H) emission band.

Attention is drawn to the nonlinear behavior of the relative intensity of the H band, which reflects the concentration of H atoms. As can be seen from the channels (1)–(5) of CH₄ fragmentation, H atoms are formed in reactions (1), (3) and (4) with the branching ratios BR = 0.5; 0.2 and 0.1, respectively, for a photon energy of 9.8 eV and BR = 0.25; 0.5 and 0.2 for a photon energy of 12.1 eV according to [79], in which an analysis of energy-dependent branching ratios, the so-called breakdown curves, was presented. Let us analyze the reactions of secondary products of methane transformation CH₃ and CH₂ based on the data [79]:



and



The emission of self-trapped excitons (9.8 eV) can produce H atoms from CH₃ via channels (6), (7) and (9) with BR = 0.28, 0.5 and 0.25, correspondingly. An excitation of CH₂ by these photons induces its dissociation via channels (10) and (11) with BR = 0.45 for both channels. In this case, 2H atoms are produced in a correlated way in channel (11). When excited by free Ar excitons (12.06 eV), the main contribution to the formation of the H atom is made by channels (6), (7) and (9) with BR = 0.2, 0.8 and 0.3, respectively; moreover, reaction (7) produces 2H atoms simultaneously. Formation of H atoms from CH₂ occurs most effectively via channel (11) with BR = 1. Channel (10) does not operate (BR = 0) at this photon energy. It should be noted that H atoms that are formed in these reactions have an excess of kinetic energy, e.g., in channel (1), the experimental mean kinetic energy of the neutral lighter fragment H appeared to be 3.1 eV [79]. In most other channels, this energy exceeds 1 eV and such “fast” H atoms may diffuse for quite a long distance facilitating H + H recombination after thermalization. The mobility of H atoms in rare gas solids and the stability of trapping sites have been the subject of numerous studies, including in [80–85]. The case of an Ar matrix was considered in [81,84]. In Ar matrices, the hydrogen

atom can occupy two types of sites—interstitial O_h and substitutional ones. According to [81], the EPR signals due to interstitially trapped hydrogen atoms in octahedral sites disappear near 16 K in solid Ar. The atoms trapped in the substitutional sites remain trapped [84]. However, their excitation via energy transfer leads to the excimers' Ar_2H^* formation and the resumption of the diffusion process. As a result, the processes of H atom production and their recombination compete with each other upon irradiation.

Our study of the dose dependences of the emission of H atoms and CH radicals performed at low temperatures showed a sharply nonmonotonic behavior of these emissions. As follows from the analysis of BR reactions (4), (7), (8) and (10), CH_3 radicals remain the main source of CH radical formation upon excitation by free excitons of the matrix; so, the conclusion that CH is a CH_3 marker [55] remains valid. Figure 6 shows the dose dependencies of the H and CH emissions measured simultaneously with the pressure in the experimental chamber.

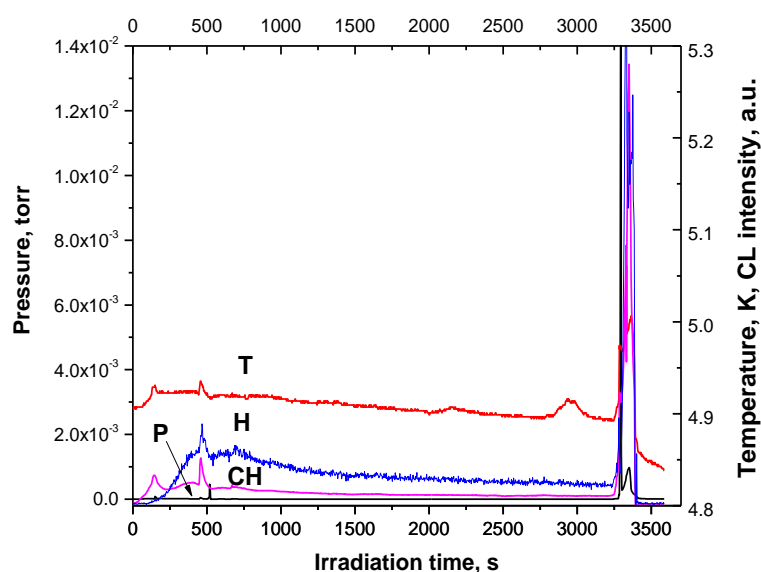


Figure 6. Dose dependencies of optical emission of H atoms and CH radicals taken from highly doped Ar matrix (C of $CH_4 = 10\%$) upon irradiation with an electron beam. This Figure also shows the dose dependencies of the pressure and temperature of the sample measured in a correlated way with optical emissions.

The dose behavior of both optical emissions was quite nonmonotonic. We first observed an increase in both optical emissions and then an exit to saturation after 350 s of exposure to an electron beam, followed by a very gradual decrease. Weak bursts on the radiation yield curves were detected—two on the curve for the CH band and one on the curve for the H band. These peaks correlated with small peaks on the temperature curve. The main change in yields occurred after 3250 s of irradiation. This phenomenon is quite similar to the observed in pure solid methane [29,43] interpreted as the result of thermo-concentration self-oscillations [44]. Details of the emission yields together with changes in temperature and pressure are shown in Figure 7a,b.

After prolonged irradiation at about 3250 s, the temperature and intensity of the H band, which is proportional to the number of H atoms in the matrix, begin to increase, and then the intensity of the H band decreases, while the temperature and pressure sharply increase. It should be noted that since the temperature sensor (Si diode) was mounted on the back of a substrate cooled by LHe, it was not possible to determine the actual surface temperature of the Ar film. However, its significant increase during explosive emission of particles is indicated by a sharp drop in the TSEE yield, measured after explosive emission and redistribution of the TSEE yield with respect to the TSEE measured after irradiation of the sample with a subcritical dose. The beginning sublimation of the sample allows one to

estimate only the lower boundary of the heating pulse—30 K. In reality, the temperature rise in the pulse exceeds the triple point temperature of Ar—87.78 K [64]. The temperature pulse has three maxima and its duration was 100 s. After the first burst of pressure, which lasted about 20 s another maximum pressure rise was observed but longer and less intense. During this period, the change in the intensity of the H band followed the temperature course. Such an unexpected, at first glance, behavior of the H band can be understood if we consider more carefully the processes of energy transfer to the products of ongoing reactions. A high temperature of the sample during the burst is a “fingerprint” of the occurrence of exothermic reactions, in particular, the reaction of H atom recombination. Transfer of energy by free excitons of the Ar matrix can populate low electronic states of H₂ molecule: the singlet state B¹Σ_u⁺ and the triplet state a³Σ_g⁺, as can be seen from Figure 8.

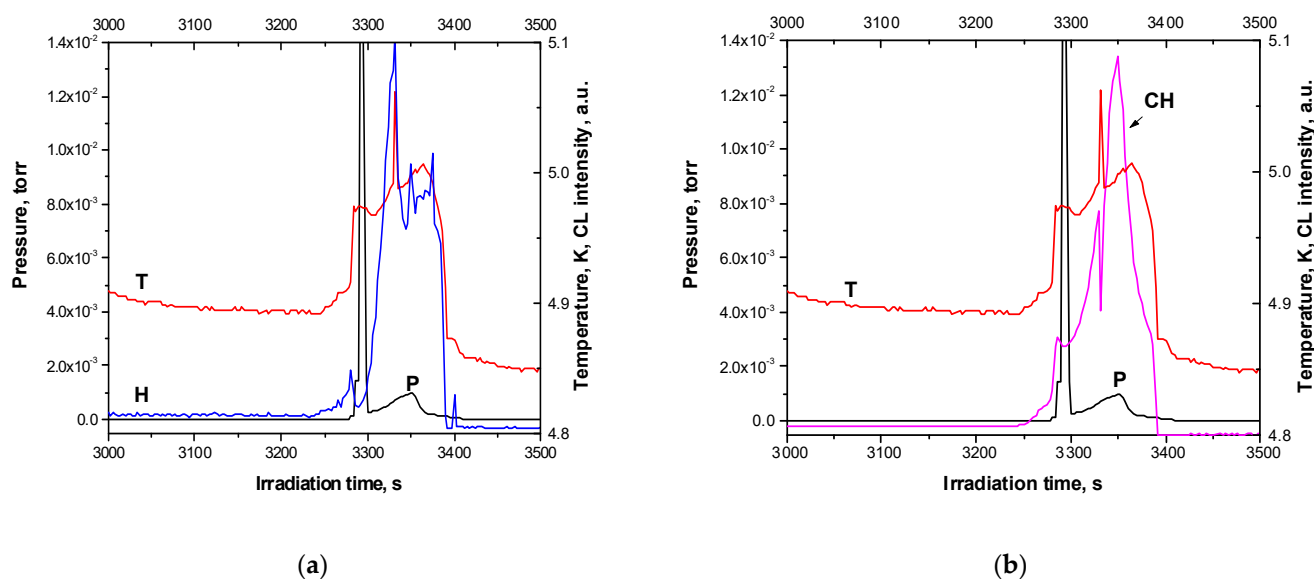


Figure 7. Yields of optical emissions in the range of pressure burst: (a) yield of the H band; (b) yield of the CH band. Both yields are recorded simultaneously with pressure and temperature.

Transitions from the bound triplet state a³Σ_g⁺ to the repulsion curve of the lower state b³Σ_u⁺ result in the dissociation of the hydrogen molecule and the appearance of two “hot” H atoms, which, after thermalization, form centers responsible for the emission of the H band. Thus, the processes of recombination of H atoms with the formation of H₂ molecules proceed in competition with the photon-induced dissociation of H₂, which affects the dose dependence of the H band. An increase in the H band intensity during a burst of pressure was also observed at a methane concentration of C = 1% in the Ar matrix [54]. However, this fact was misinterpreted as the absence of a contribution from the recombination of H atoms to the delayed desorption, since long before the pressure burst in this experiment, we observed a sharp drop in the intensity of the H band, which was attributed to the recombination of H atoms.

Note that the dose dependences of the H band intensity measured on lightly (C = 1%) and highly (C = 10%) doped matrices are different. While in the case of a highly doped Ar matrix, the burst was observed after the stage of a slow decrease in the intensity of the H band (see Figure 6), in the case of a lightly doped matrix, the burst followed its growth as shown in Figure 9. The decrease in the burst delay time in this experiment is associated with the use of higher current density.

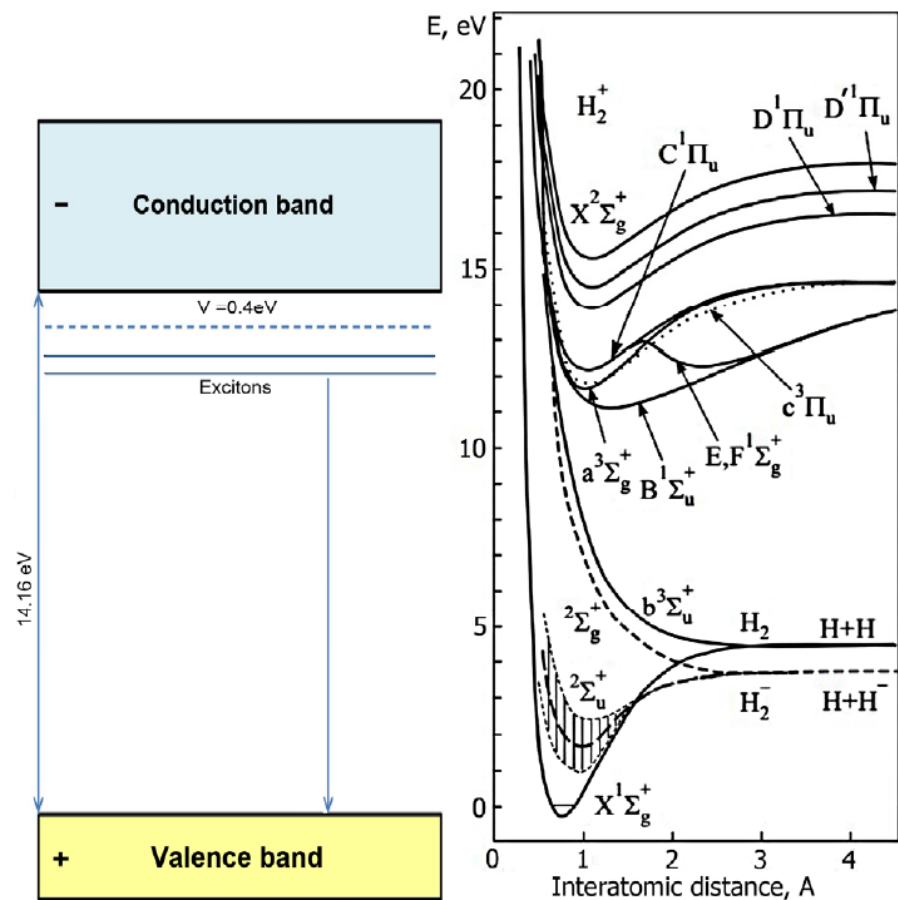


Figure 8. Energy scheme of Ar and potential curves of H_2 , H_2^+ [86] and H_2^- [87].

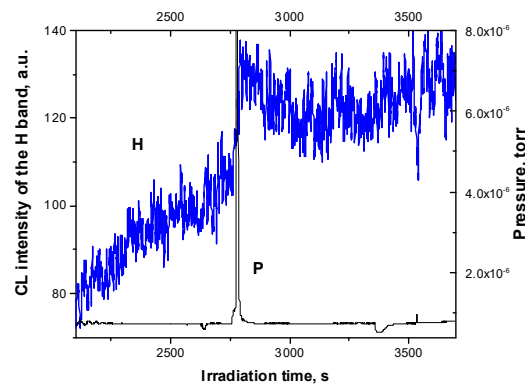


Figure 9. Dose dependence of the H band detected in a correlated manner with the total yield of particle (P) from lightly doped Ar matrix ($C = 1\%$ of CH_4). Irradiation was performed with a 1.5 keV electron beam at current density of 3 mAcm^{-1} .

At a methane concentration of $C = 5\%$, the dose dependence of the H band is similar to that recorded for 1%. It should be noted that the concentration of the radiolysis products is significantly lower than that of the dopant since many different primary dissociation channels operate simultaneously. Due to this, the conditions for excitation of H_2 by free excitons change with concentration: with increasing C , the efficiency of excitation of H_2 by excitons rises and therefore the contribution of the recombination reaction of H atoms to the H band increases. Accordingly, the flash effect accompanying the ejection of particles appeared to be much more pronounced at 10%, as can be seen from the comparison of Figures 7a and 9. It should be noted that in lightly doped matrices at $C = 0.1\%$ of methane,

no explosive ejection of particles and flashes was observed, which determines the critical concentration for these phenomena as $C = 1\%$.

It is interesting to compare the dose dependence of the H band with that detected for the CH band in a highly doped matrix (see Figures 6 and 7b). An intensity of the CH band, which is a marker of the CH_3 radical, follows the temperature course with the exception of one local event at about 3340 s when the temperature and intensity of the CH band change in the opposite way. Such a behavior became clear if we consider the balance and interplay between C_2H_6 and CH_3 . As follows from Refs. [63,88,89], the photodissociation (absorption) cross-section of ethane is close to that of methane and both free and self-trapped excitons fall into the range of ethane absorption. There are a number of primary dissociation channels which include reactions: $\text{C}_2\text{H}_6 + h\nu \rightarrow \text{CH}_3 + \text{CH}_3$ and $\text{C}_2\text{H}_6 + h\nu \rightarrow \text{CH}_3^* + \text{CH}_3$ [88]. Note that the enthalpy $\Delta_r H$ of the second reaction with the excited CH_3^* radical formation $\Delta_r H = 9.54$ eV [88], is close to the photon energy of self-trapped excitons in Ar (9.8 eV). The enthalpy of the first reaction is essentially lower— $\Delta_r H = 3.81$ eV [88], and both of them can proceed. Unfortunately, at present, to the best of our knowledge, there is no quantitative information on the branching ratios of these reactions; however, as it was shown [88], the reaction with C-C bond fission yielding two CH_3 radicals refers to active channels of the C_2H_6 photodissociation. Based on this conclusion, we can expect similar behavior of the CH and H bands during the burst. The results obtained (see Figure 7a,b) suggest that the luminescence flashes detected in these bands can be assigned as indicators of the recombination of H atoms and CH_3 radicals with the release of thermal energy, which ensures the explosive ejection of particles. These results agree with the data of [52], where the delayed recombination of CH_3 radicals was observed by the FTIR method upon irradiation of a mixture of methane and carbon monoxide with fast electrons (5 keV). These authors also observed some sharp pressure rise in the process.

4. Conclusions

The influence of the environment on the radiation-induced processes in Ar matrices doped with methane ($C = 0.1\text{--}10\%$) was studied by means of emission spectroscopy methods. Electrons of subthreshold energy (1.5 keV) were used to eliminate the knock-on defect formation and desorption. The TSEE study of charge accumulation in Ar and CH_4 -doped matrices provided evidence against the “Coulomb explosion” scenario as the underlying mechanism for explaining the delayed explosive ejection of particles under the beam. Four products of methane transformation were detected—H and C atoms and H_2 molecules and CH radicals. Analysis of methane transformation reactions induced by free and self-trapped excitons showed that the CH radical can be considered a marker of the CH_3 species. Three channels of energy transfer to dopant and radiolysis products were considered: free holes, free excitons and photons from the “intrinsic source” provided by the emission of the self-trapped excitons. Special attention was paid to the dynamics of radiolysis products—H atoms, H_2 molecules and CH_3 radicals (via CH species). Dose dependencies of the radiolysis products along with the total yield of desorbing particles were monitored in a correlated manner. The competition between exciton self-trapping and energy transfer to the dopant and radiolysis products has been analyzed. A nonlinear concentration behavior of the H atoms in doped Ar matrices has been established. The study revealed a nonmonotonic behavior of the optical yields of H atoms and CH radicals with a strong luminescence flash (after nearly an hour of irradiation), which correlated with the temperature surge and explosive pulse of particle ejection. An analysis of the energy transfer and trapping processes made it possible to explain the seemingly contradictory observation of a surge in the optical emission of H atoms and CH_3 radicals as an indicator of their recombination. Thus, this study provided spectroscopic evidence for both atomic and radical recombination reactions proceeding without external heating when accumulated to a critical concentration as the basis for the delayed explosive ejection of particles during irradiation. The further step would be to extend this research to other chemical compounds.

Author Contributions: E.S.: conceptualization, writing—original draft, review and editing, and supervision. I.K.: investigation, software, and validation. S.U.: investigation and methodology. M.B.: investigation and resources. All authors have read and agreed to the published version of the manuscript.

Funding: This research received no external funding.

Institutional Review Board Statement: The study did not require ethical approval.

Informed Consent Statement: The study did not involve humans.

Data Availability Statement: All the information obtained was included in the article.

Acknowledgments: The authors cordially thank their colleagues Vladimir Sugakov, Oleg Kirichek, Robert Kolos, Claudine Crepin-Gilbert, Hermann Rothard, Anatoli Popov and Giovanni Strazzulla, for stimulating discussions.

Conflicts of Interest: The authors declare no conflict of interest.

References

1. Clark, R.N.; Carlson, R.; Grundy, W.; Noll, K. Observed Ices in the Solar System. In *The Science of Solar System Ices*; Gudipati, M.S., Castillo-Rogez, J., Eds.; Astrophysics and Space Science Library; Springer: New York, NY, USA, 2012; Volume 356, pp. 3–46. [[CrossRef](#)]
2. Boogert, A.C.A.; Gerakines, P.A.; Whittet, D.C.B. Observation of the Icy Universe. *Annu. Rev. Astron. Astrophys.* **2015**, *53*, 541–581. [[CrossRef](#)]
3. Guzmán-Marmolejo, A.; Segura, A. Methane in the Solar System. *Boletín Soc. Geológica Mex.* **2015**, *67*, 377–385. [[CrossRef](#)]
4. Lacy, J.H.; Carr, J.S.; Evans, N.J.; Baas, F.; Achtermann, J.M.; Arens, J.F. Discovery of interstellar methane: Observations of gaseous and solid CH₄ absorption toward young stars in molecular clouds. *Astrophys. J.* **1991**, *376*, 556–560. [[CrossRef](#)]
5. Cruikshank, D.P.; Brown, R.H.; Calvin, W.M.; Roush, T.L.; Bartholomew, M.J. Ices on the satellites of Jupiter, Saturn, and Uranus. In *Solar System Ices*; Schmitt, B., de Bergh, C., Eds.; Kluwer Academic: Dordrecht, The Netherlands, 1998; pp. 579–606.
6. Gibb, E.L.; Mumma, M.J.; Dello Russo, N.; DiSanti, M.A.; Magee-Sauer, K. Methane in Oort cloud comets. *Icarus* **2003**, *165*, 391–406. [[CrossRef](#)]
7. Öberg, K.I. Photochemistry and astrochemistry: Photochemical pathways to interstellar complex organic molecules. *Chem. Rev.* **2016**, *116*, 9631–9663. [[CrossRef](#)] [[PubMed](#)]
8. Kobayashi, K.; Geppert, W.D.; Carrasco, N.; Holm, N.G.; Mousis, O.; Palumbo, M.E.; Waite, J.H.; Watanabe, N.; Ziurys, L.M. Laboratory studies of methane and its relationship to prebiotic chemistry. *Astrobiology* **2017**, *17*, 786–812. [[CrossRef](#)] [[PubMed](#)]
9. Allodi, M.A.; Baragiola, R.A.; Baratta, G.A.; Barucci, M.A.; Blake, G.A.; Brucato, J.R.; Contreras, C.; Cuyllé, S.H.; Boduch, P.; Fulvio, D.; et al. Complementary and Emerging Techniques for Astrophysical Ices Processed in the Laboratory. *Space Sci. Rev.* **2013**, *180*, 101–175. [[CrossRef](#)]
10. Foti, G.; Calcagno, L.; Sheng, K.L.; Strazzulla, G. Micrometre-sized polymer layers synthesized by MeV ions impinging on frozen methane. *Nature* **1984**, *310*, 126–128. [[CrossRef](#)]
11. Kaiser, R.I.; Roessler, K. Theoretical and laboratory study on the interaction of cosmic-ray particles with interstellar ices. III. Suprathermal chemistry-induced formation of hydrocarbon molecules in solid methane (CH₄), ethylene (C₂H₄) and acetylene (C₂H₂). *Astrophys. J.* **1998**, *503*, 959–975. [[CrossRef](#)]
12. Brunetto, R.; Barucci, M.A.; Dotto, E.; Strazzulla, G. Ion Irradiation of Frozen Methanol, Methane, and Benzene: Linking to the Colors of Centaurs and Trans-Neptunian Objects. *Astrophys. J.* **2006**, *644*, 646–650. [[CrossRef](#)]
13. Palumbo, M.E.; Baratta, G.A.; Fulvio, D.; Garozzo, M.; Gomis, O.; Leto, G.; Spinella, F.; Strazzulla, G. Ion irradiation of astrophysical ices. *J. Phys. Conf. Ser.* **2008**, *101*, 012002. [[CrossRef](#)]
14. Ennis, C.; Yuan, H.; Sibener, S.J.; Kaiser, R.I. On the chemical processing of hydrocarbon surfaces by fast oxygen ions. *Phys. Chem. Chem. Phys.* **2011**, *13*, 17870–17884. [[CrossRef](#)] [[PubMed](#)]
15. de Barros, A.L.F.; Bordalo, V.; Duarte, E.S.; de Silveira, E.F.; Domaracka, A.; Rothard, H.; Boduch, P. Cosmic ray impact on astrophysical ices: Laboratory studies on heavy ion irradiation of methane. *Astron. Astrophys.* **2011**, *531*, A160. [[CrossRef](#)]
16. Mejía, C.F.; de Barros, A.L.F.; Bordalo, V.; da Silveira, E.F.; Boduch, P.; Domaracka, A.; Rothard, H. Cosmic ray–ice interaction studied by radiolysis of 15 K methane ice with MeV O, Fe and Zn ions. *Mon. Not. R. Astron. Soc.* **2013**, *433*, 2368–2379. [[CrossRef](#)]
17. Boduch, P.; Dartois, E.; de Barros, A.L.F.; da Silveira, E.F.; Domaracka, A.; Lv, X.-Y.; Palumbo, M.E.; Pilling, S.; Rothard, H.; Duarte, E.S.; et al. Radiation effects in astrophysical ices. *J. Phys. Conf. Ser.* **2015**, *629*, 012008. [[CrossRef](#)]
18. Vasconcelos, F.A.; Pilling, S.; Rocha, W.R.M.; Rothard, H.; Boduch, P.; Ding, J.J. Ion irradiation of pure and amorphous CH₄ ice relevant for astrophysical environments. *Phys. Chem. Chem. Phys.* **2017**, *19*, 12845–12856. [[CrossRef](#)] [[PubMed](#)]
19. Mejía, C.; de Barros, A.L.F.; Rothard, H.; Boduch, P.; da Silveira, E.F. Radiolysis of Ices by Cosmic-Rays: CH₄ and H₂O Ices Mixtures Irradiated by 40 MeV ⁵⁸Ni¹¹⁺ Ions. *Astrophys. J.* **2020**, *894*, 132. [[CrossRef](#)]
20. Huang, T.; Hamill, W.H. Characteristic energy loss, luminescence and luminescence excitation spectra of methane and other alkane solids under low-energy electron impact. *J. Phys. Chem.* **1974**, *78*, 2077–2080. [[CrossRef](#)]

21. Bennett, C.J.; Jamieson, C.S.; Osamura, Y.; Kaiser, R.I. Laboratory studies on the irradiation of methane in interstellar, cometary, and solar system ices. *Astrophys. J.* **2006**, *653*, 792–811. [[CrossRef](#)]
22. Barberio, M.; Vasta, R.; Barone, P.; Manicò, G.; Xu, F. Experimental and theoretical study on the ethane and acetylene formation from electron irradiation of methane ices. *World J. Condens. Matter Phys.* **2013**, *3*, 14–20. [[CrossRef](#)]
23. Huels, M.A.; Parenteau, L.; Bass, A.D.; Sanche, L. Small steps on the slippery road to life: Molecular synthesis in astrophysical ices initiated by low energy electron impact. *Int. J. Mass Spectrom.* **2008**, *277*, 256–261. [[CrossRef](#)]
24. Jones, B.M.; Kaiser, R.I. Application of reflectron time-of-flight mass spectroscopy in the analysis of astrophysically relevant ices exposed to ionization radiation: Methane (CH₄) and D₄-methane (CD₄) as a case study. *J. Phys. Chem. Lett.* **2013**, *4*, 1965–1971. [[CrossRef](#)] [[PubMed](#)]
25. Materese, C.K.; Cruikshank, D.P.; Sandford, S.A.; Imanaka, H.; Nuevo, M. Ice chemistry on outer Solar System bodies: Electron radiolysis of N₂-, CH₄-, and CO-containing ices. *Astrophys. J.* **2015**, *812*, 150. [[CrossRef](#)] [[PubMed](#)]
26. Abplanalp, M.J.; Jones, B.M.; Kaiser, R.I. Untangling the methane chemistry in interstellar and solar system ices toward ionizing radiation: A combined infrared and reflectron time-of-flight analysis. *Phys. Chem. Chem. Phys.* **2018**, *20*, 5435–5468. [[CrossRef](#)] [[PubMed](#)]
27. Savchenko, E.; Khyzhniy, I.; Uytunov, S.; Bludov, M.; Barabashov, A.; Gumenchuk, G.; Bondybey, V. Radiation effects in nitrogen and methane “ices”. *Nucl. Instr. Meth. B* **2018**, *435*, 38–42. [[CrossRef](#)]
28. Savchenko, E.V.; Kirichek, O.; Lawson, C.R.; Khyzhniy, I.V.; Uytunov, S.A.; Bludov, M.A. Relaxation processes in solid methane pre-irradiated with an electron beam. *Nucl. Instrum. Meth. B* **2018**, *433*, 23–27. [[CrossRef](#)]
29. Savchenko, E.; Khyzhniy, I.; Uytunov, S.; Bludov, M.; Gumenchuk, G.; Bondybey, V. Effects induced by an electron beam in methane ices. *Nucl. Instrum. Meth. B* **2019**, *460*, 244–248. [[CrossRef](#)]
30. Hodyss, R.; Johnson, P.V.; Stern, J.V.; Goguen, J.D.; Kanik, I. Photochemistry of methane-water ices. *Icarus* **2009**, *200*, 338–342. [[CrossRef](#)]
31. Hodyss, R.; Howard, H.R.; Johnson, P.V.; Goguen, J.D.; Kanik, I. Formation of radical species in photolyzed CH₄:N₂ ices. *Icarus* **2011**, *214*, 748–753. [[CrossRef](#)]
32. Wu, Y.-J.; Wu, C.Y.R.; Chou, S.-L.; Lin, M.-Y.; Lu, H.-C.; Lo, J.-I.; Cheng, B.-M. Spectra and photolysis of pure nitrogen and methane dispersed in solid nitrogen with vacuum-ultraviolet light. *Astrophys. J.* **2012**, *746*, 175. [[CrossRef](#)]
33. Bossa, J.-B.; Paardekooper, D.M.; Isokoski, K.; Linnartz, H. Methane ice photochemistry and kinetic study using laser desorption time-of-flight mass spectrometry at 20 K. *Phys. Chem. Chem. Phys.* **2015**, *17*, 17346–17354. [[CrossRef](#)] [[PubMed](#)]
34. Dupuy, R.; Bertin, M.; Féraud, G.; Michaut, X.; Jeseck, P.; Doronin, M.; Philippe, L.; Romanzin, C.; Fillion, J.-H. Spectrally-resolved UV photodesorption of CH₄ in pure and layered ices. *Astron. Astrophys.* **2017**, *603*, A61. [[CrossRef](#)]
35. Krim, L.; Jonusas, M. VUV Photolysis of CH₄-H₂O mixture in methane-rich ices: Formation of large complex organic molecules in astronomical environments. *Low Temp. Phys./Fiz. Nizk. Temp.* **2019**, *45*, 606–614. [[CrossRef](#)]
36. Scott, T.L.; Carpenter, J.M.; Miller, M.E. The development of solid methane neutron moderators at the intense pulsed neutron source facility of Argonne National Laboratory. *Preprint*, 1999; ANL/IPNS/CP-98533.
37. Carpenter, J.M. Thermally activated release of stored chemical energy in cryogenic media. *Nature* **1987**, *330*, 358–360. [[CrossRef](#)]
38. Kulagin, E.; Kulikov, S.; Melikhov, V.; Shabalin, E. Radiation effects in cold moderator materials: Experimental study of accumulation and release of chemical energy. *Nucl. Instrum. Methods B* **2004**, *215*, 181–186. [[CrossRef](#)]
39. Feng, Q.X.; Feng, Q.K.; Kawai, T.; Zhong, B.; Wei, J.; Loong, C.-K.; Liang, T.J. The Solution of Cold Neutron Source using Solid Methane Moderator for the CPHS. *Phys. Procedia* **2012**, *26*, 49–54. [[CrossRef](#)]
40. Kirichek, O.; Lawson, C.R.; Jenkins, D.M.; Ridley, C.J.T.; Haynes, D.J. Solid methane in neutron radiation: Cryogenic moderators and cometary cryovolcanism. *Cryogenics* **2017**, *88*, 101–105. [[CrossRef](#)]
41. Kirichek, O.; Savchenko, E.V.; Lawson, C.R.; Khyzhniy, I.V.; Jenkins, D.M.; Uytunov, S.A.; Bludov, M.A.; Haynes, D.J. Recombination of radiation defects in solid methane: Neutron sources and cryo-volcanism on celestial bodies. *J. Phys. Conf. Ser.* **2018**, *969*, 012006. [[CrossRef](#)]
42. Kirichek, O.; Lawson, C.R.; Draper, G.L.; Jenkins, D.M.; Haynes, D.J.; Lilley, S. Solid methane moderators: Thermodynamics and chemistry. *J. Neutron Res.* **2020**, *22*, 281–286. [[CrossRef](#)]
43. Khyzhniy, I.V.; Uytunov, S.A.; Bludov, M.A.; Savchenko, E.V. Explosive particle desorption from solid methane induced by an electron beam. *Low Temp. Phys./Fiz. Nizk. Temp.* **2018**, *44*, 1223–1225. [[CrossRef](#)]
44. Bludov, M.A.; Khyzhniy, I.V.; Savchenko, E.V.; Sugakov, V.I.; Uytunov, S.A. Self-oscillations in solid methane irradiated by electrons. *Nucl. Phys. At. Energy* **2020**, *21*, 312–322. [[CrossRef](#)]
45. Sugakov, V.I. *Lectures in Synergetics, World Scientific Series on Nonlinear Science*; World Scientific: Singapore, 1998; Volume 33.
46. Brown, W.L.; Foti, G.; Lanzerotti, L.J.; Bower, J.E.; Johnson, R.E. Delayed emission of hydrogen from ion bombardment of solid methane. *Nucl. Instrum. Methods B* **1987**, *19–20*, 899–902. [[CrossRef](#)]
47. Kaiser, R.I.; Eich, G.; Gabrysch, A.; Roessler, K. Theoretical and laboratory studies on the interaction of cosmic-ray particles with interstellar ices. II. Formation of atomic and molecular hydrogen in frozen organic molecules. *Astrophys. J.* **1997**, *484*, 487–498. [[CrossRef](#)]
48. d’Hendecourt, L.; Allamandola, L.; Baas, F.; Greenberg, J. Interstellar grain explosions—Molecule cycling between gas and dust. *Astron. Astrophys.* **1982**, *109*, L12–L14.

49. Roberts, J.; Rawlings, J.; Viti, S.; Williams, D. Desorption from interstellar ices. *Mon. Not. R. Astron. Soc.* **2007**, *382*, 733–742. [[CrossRef](#)]
50. Vasyunin, A.; Herbst, E. Reactive desorption and radiative association as possible drivers of complex molecule formation in the cold interstellar medium. *Astrophys. J.* **2013**, *769*, 34. [[CrossRef](#)]
51. Wakelam, V.; Dartois, E.; Chabot, M.; Spezzano, S.; Navarro-Almaida, D.; Loison, J.-C.; Fuente, A. Efficiency of non-thermal desorptions in cold-core conditions: Testing the sputtering of grain mantles induced by cosmic rays. *Astron. Astrophys.* **2021**, *652*, A63. [[CrossRef](#)]
52. Zhu, C.; Bergantini, A.; Singh, S.K.; Abplanalp, M.J.; Kaiser, R.I. Rapid radical–radical induced explosive desorption of ice-coated interstellar nanoparticles. *Astrophys. J.* **2021**, *920*, 73. [[CrossRef](#)]
53. Khyzhniy, I.V.; Uytunov, S.A.; Bludov, M.A.; Savchenko, E.V.; Bondybey, V.E. Electron-induced delayed desorption of solid argon doped with methane. *Low Temp. Phys./Fiz. Nizk. Temp.* **2019**, *45*, 721–726. [[CrossRef](#)]
54. Savchenko, E.; Khyzhniy, I.; Uytunov, S.; Bludov, M.; Bondybey, V. Explosive desorption from solid methane and methane-containing Argon matrices. *Nucl. Instrum. Meth. B* **2020**, *469*, 37–41. [[CrossRef](#)]
55. Savchenko, E.V.; Khyzhniy, I.V.; Uytunov, S.A.; Bludov, M.A.; Bondybey, V.E. Nonstationary processes in matrix-isolated methane probed by optical and current emission spectroscopy. *J. Mol. Struct.* **2020**, *1221*, 128803. [[CrossRef](#)]
56. Eberlein, J.; Creuzburg, M. Dissociation of CH₄ in a krypton matrix: VUV spectra of atomic C and of the radical CH. *Mol. Phys.* **1999**, *96*, 451–456. [[CrossRef](#)]
57. Wu, Y.-J.; Chen, H.-F.; Camacho, C.; Witek, H.A.; Hsu, S.-C.; Lin, M.-Y.; Chou, S.-L.; Ogilvie, J.F.; Cheng, B.-M. Formation and identification of interstellar molecule linear C₅H from photolysis of methane dispersed in solid neon. *Astrophys. J.* **2009**, *701*, 8–11. [[CrossRef](#)]
58. Lin, M.-Y.; Lo, J.-I.; Lu, H.-C.; Chou, S.-L.; Peng, Y.-C.; Cheng, B.-M.; Ogilvie, J.F. Vacuum-Ultraviolet photolysis of methane at 3 K: Synthesis of carbon clusters up to C₂₀. *J. Phys. Chem. A* **2014**, *118*, 3438–3449. [[CrossRef](#)] [[PubMed](#)]
59. Savchenko, E.; Khyzhniy, I.; Uytunov, S.; Bludov, M.; Bondybey, V. Explosive desorption induced by radical-radical interaction in methane-doped Ar matrices. *Nucl. Instr. Meth. B* **2023**, *536*, 113–118. [[CrossRef](#)]
60. Sharp, T.E. Potential-Energy Curves for Molecular Hydrogen and its Ions. *At. Data* **1971**, *2*, 119–169. [[CrossRef](#)]
61. Song, K.S.; Williams, R.T. *Self-Trapped Excitons*; Springer: Berlin/Heidelberg, Germany, 1996.
62. Smirnov, B.M.; Yatsenko, A.S. Properties of dimers. *Phys. Usp.* **1996**, *39*, 211–230. [[CrossRef](#)]
63. Heays, A.N.; Bosman, A.D.; van Dishoeck, E.F. Photodissociation and photoionisation of atoms and molecules. *Astron. Astrophys.* **2017**, *602*, A105. [[CrossRef](#)]
64. NIST Chemistry WebBook. Available online: <https://webbook.nist.gov/chemistry/> (accessed on 30 July 2023).
65. Ismail, A.F.; Khulbe, K.C.; Matsuura, T. *Gas Separation Membranes: Polymeric and Inorganic*; Springer: Berlin/Heidelberg, Germany, 2015.
66. Hallam, H.E. (Ed.) *Vibrational Spectroscopy of Trapped Species*; John Wiley & Sons: London, UK, 1973.
67. Chamberland, A.; Belzile, R.; Cabana, A. Infrared spectra and structure of methane—Noble gas mixed crystals: The influence of temperature and methane concentration on the ν₃ vibration band of methane. *Canadian J. Chem.* **1970**, *48*, 1129–1139. [[CrossRef](#)]
68. Ferradini, C.; Jay-Gerin, J.-P. *Excess Electrons in Dielectric Media*; CRC Press: Boca Raton, FL, USA; Ann Arbor, MI, USA; Boston, MA, USA; London, UK, 1991.
69. Lo, J.-I.; Lin, M.-Y.; Peng, Y.-C.; Chou, S.-L.; Lu, H.-C.; Cheng, B.-M.; Ogilvie, J.F. Far-ultraviolet photolysis of solid methane. *Mon. Not. R. Astron. Soc.* **2015**, *451*, 159–166. [[CrossRef](#)]
70. Kraas, M.; Gürtler, P. Emission and excitation spectra of rare gas hydride trimers in rare gas matrices. *Chem. Phys. Lett.* **1990**, *174*, 396–400. [[CrossRef](#)]
71. Doronin, Y.S.; Vakula, V.L.; Kamarchuk, G.V.; Tkachenko, A.A.; Khyzhniy, I.V.; Uytunov, S.A.; Bludov, M.A.; Savchenko, E.V. Desorption of excited H* atoms from free clusters Ar/CH₄ and solid Ar doped with CH₄. *Low Temp. Phys./Fiz. Nizk. Temp.* **2021**, *47*, 1058–1064. [[CrossRef](#)]
72. Zimmerer, G. Electronic sputtering from rare-gas solids. *Nucl. Instrum. Methods B* **1994**, *91*, 601–613. [[CrossRef](#)]
73. Gumenchuk, G.B.; Khyzhniy, I.V.; Belov, A.G.; Ponomaryov, A.N.; Savchenko, E.V.; Bludov, M.A.; Uytunov, S.A.; Bondybey, V.E. Optically stimulated desorption of “hot” molecules from pre-irradiated Ar solids. *Low Temp. Phys./Fiz. Nizk. Temp.* **2008**, *34*, 241–244. [[CrossRef](#)]
74. Ogurtsov, A.N.; Savchenko, E.V.; Becker, J.; Runne, M.; Zimmerer, G. Radiative relaxation of optically generated intrinsic charged centers in solid Ar. *J. Lumin.* **1998**, *76–77*, 478–481. [[CrossRef](#)]
75. Lavrov, B.P.; Melnikov, A.S.; Käning, M.; Röpkcke, J. UV continuum emission and diagnostics of hydrogen-containing non-equilibrium plasmas. *Phys. Rev. E* **1999**, *59*, 3526–3543. [[CrossRef](#)]
76. Coletti, A.F.; Debever, J.M.; Zimmerer, G. Electron stimulated desorption of solid argon via exciton creation. *J. Phys. Lett. Edp. Sci.* **1984**, *45*, 467–473. [[CrossRef](#)]
77. Fugol, I.Y. Free and self-trapped excitons in cryocrystals: Kinetics and relaxation processes. *Adv. Phys.* **1988**, *37*, 1–35. [[CrossRef](#)]
78. Beyer, M.; Lammers, A.; Savchenko, E.V.; Niedner-Schatteburg, G.; Bondybey, V.E. Proton solvated by noble-gas atoms: Simplest case of a solvated ion. *Phys. Chem. Chem. Phys.* **1999**, *1*, 2213–2221. [[CrossRef](#)]

79. IdBarkach, T.; Chabot, M.; Béroff, K.; Della Negra, S.; Lesrel, J.; Geslin, F.; Le Padellec, A.; Mahajan, T.; Díaz-Tendero, S. Breakdown curves of $\text{CH}_2^{(+)}$, $\text{CH}_3^{(+)}$, and $\text{CH}_4^{(+)}$ molecules I. Construction and application to electron collisions and UV photodissociation. *Astron. Astrophys.* **2019**, *628*, A75. [[CrossRef](#)]
80. Eberlein, J.; Creuzburg, M. Mobility of atomic hydrogen in solid krypton and xenon. *J. Chem. Phys.* **1997**, *106*, 2188–2194. [[CrossRef](#)]
81. Vaskonen, K.; Eloranta, J.; Kiljunen, T.; Kunttu, H. Thermal mobility of atomic hydrogen in solid argon and krypton matrices. *J. Chem. Phys.* **1999**, *110*, 2122–2128. [[CrossRef](#)]
82. Kiljunen, T.; Eloranta, J.; Kunttu, H. *Ab initio* and molecular-dynamics studies on rare gas hydrides: Potential-energy curves, isotropic hyperfine properties, and matrix cage trapping of atomic hydrogen. *J. Chem. Phys.* **1999**, *110*, 11814–11822. [[CrossRef](#)]
83. Feldman, V.I.; Sukhov, F.F.; Orlov, A.Y. Hydrogen atoms in solid xenon: Trapping site structure, distribution, and stability as revealed by EPR studies in monoisotopic and isotopically enriched xenon matrices. *J. Chem. Phys.* **2008**, *128*, 214511. [[CrossRef](#)] [[PubMed](#)]
84. Oserov, G.K.; Bezrukov, D.S.; Buchachenko, A.A. Computational study of the stable atomic trapping sites in Ar lattice. *Low Temp. Phys./Fiz. Nizk. Temp.* **2019**, *45*, 301–309. [[CrossRef](#)]
85. Sheludiakov, S.; Ahokas, J.; Järvinen, J.; Lehtonen, L.; Vasiliev, S.; Dmitriev, Y.A.; Lee, D.M.; Khmelenko, V.V. Electron spin resonance study of atomic hydrogen stabilized in solid neon below 1 K. *J. Low Temp. Phys.* **2019**, *195*, 365–377. [[CrossRef](#)]
86. Sawada, K.; Fujimoto, T. Effective ionization and dissociation rate coefficients of molecular hydrogen in plasma. *J. Appl. Phys.* **1995**, *78*, 2913–2924. [[CrossRef](#)]
87. Massey, H. *Negative Ions*; Cambridge University Press: Cambridge, UK, 1976.
88. Chang, Y.; Yang, J.; Chen, Z.; Zhang, Z.; Yu, Y.; Li, Q.; He, Z.; Zhang, W.; Wu, G.; Ingle, R.A.; et al. Ultraviolet photochemistry of ethane: Implications for the atmospheric chemistry of the gas giants. *Chem. Sci.* **2020**, *11*, 5089–5097. [[CrossRef](#)]
89. Gao, H. Molecular photodissociation in the vacuum ultraviolet region: Implications for astrochemistry and planetary atmospheric chemistry. *Mol. Phys.* **2021**, *119*, e1861354. [[CrossRef](#)]

Disclaimer/Publisher's Note: The statements, opinions and data contained in all publications are solely those of the individual author(s) and contributor(s) and not of MDPI and/or the editor(s). MDPI and/or the editor(s) disclaim responsibility for any injury to people or property resulting from any ideas, methods, instructions or products referred to in the content.